Supporting Information

Enhanced Dielectric Energy Storage in Multilayer Films via Valley-type Structure Design

Tian-Yi Hu[a], Yiqin Lu[a], Yunbo Zhang[a], Chunrui Ma[a,*], Shao-Dong Cheng[b], Guangliang Hu[b], Ming Liu[b].

[a] *State Key Laboratory for Mechanical Behavior of Materials and School of Materials Science and Engineering, Xi'an Jiaotong University, Xi'an, 710049, China*

[b] *School of Microelectronics, Xi'an Jiaotong University, Xi'an,710049, China*

* Corresponding authors:

E-mail addresses: chunrui.ma@xjtu.edu.cn (C.R. Ma).

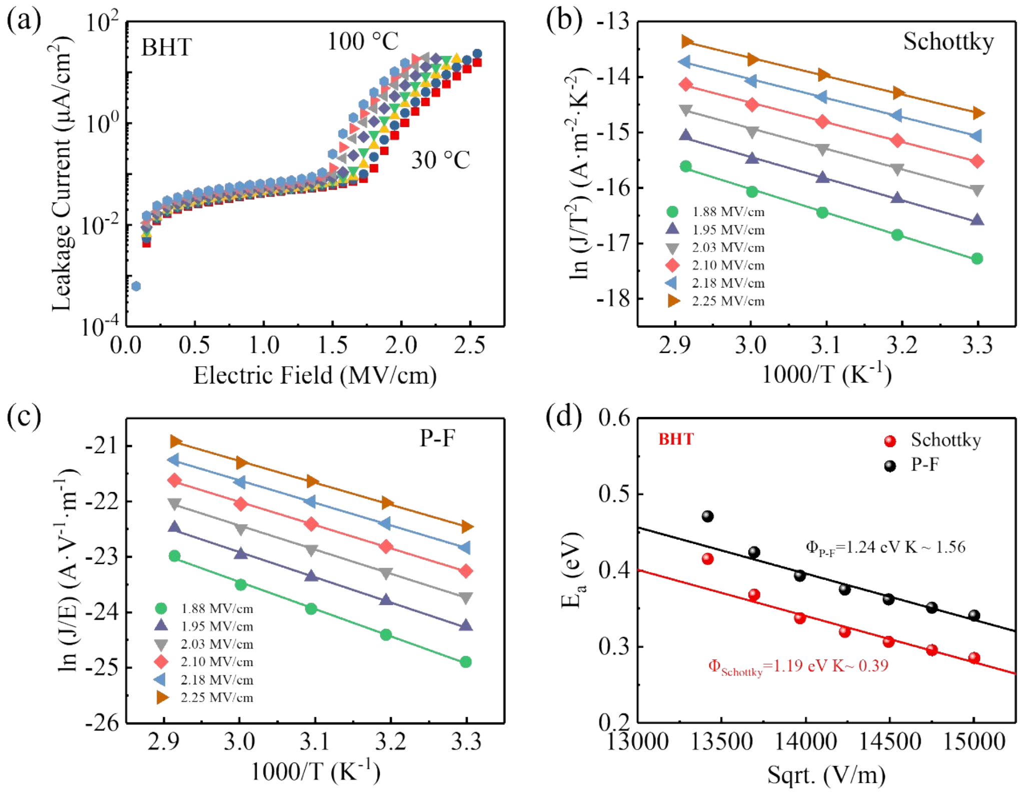

Fig S1 (a) Leakage current of the BHT thin films as a function of electric field under different temperature. Linear fittings of the temperature-dependent leakage currents to extract thermal activation energies (E_a) based on **(b)** Schottky emission and **(c)** P-F emission mechanisms. **(d)** Plots of E_a values to extrapolate the barriers height ($\Phi_{P\text{-}F}$ and $\Phi_{Schottky}$). The fitted mathematical formulas and interpretations of the mechanisms can be found in ref 1. [1]

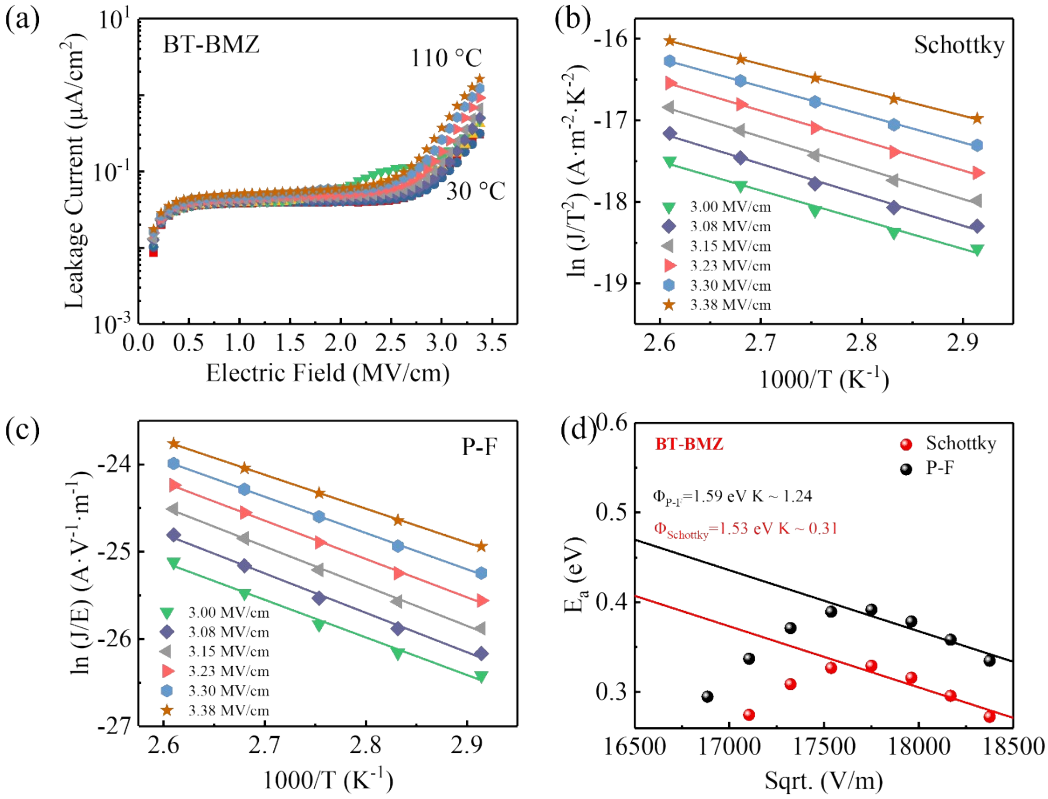

Fig S2 **(a)** Leakage current of the BT-BMZ thin films as a function of electric field under different temperature. Linear fittings of the temperature-dependent leakage currents to extract thermal activation energies (E_a) based on **(b)** Schottky emission and **(c)** P-F emission mechanisms. **(d)** Plots of E_a values to extrapolate the barriers height ($\Phi_{P\text{-}F}$ and $\Phi_{Schottky}$). The fitted mathematical formulas and interpretations of the mechanisms can be found in ref 1. [1]

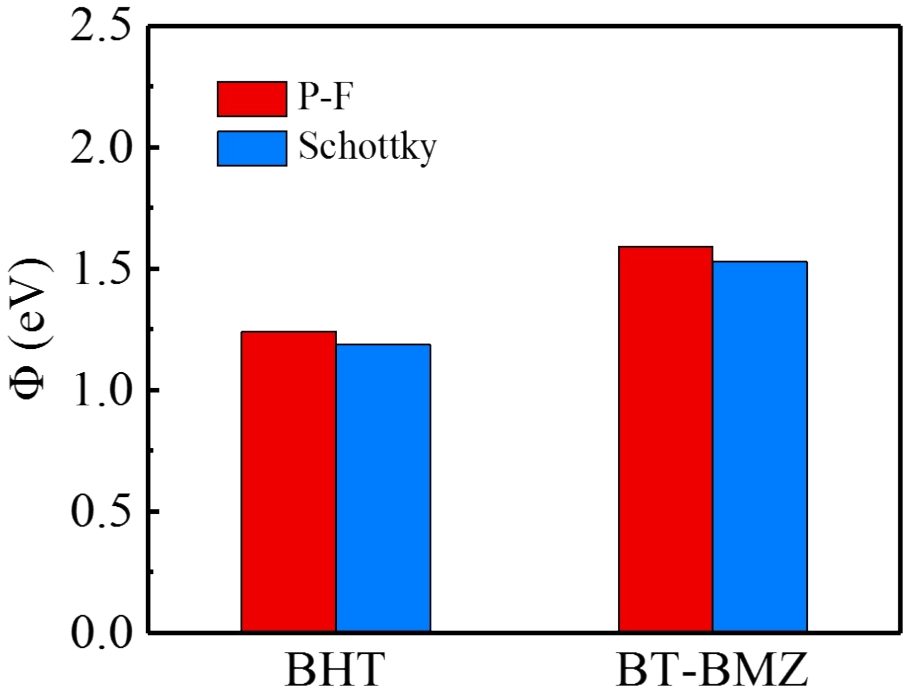

Fig S3 P-F barrier height and Schottky barrier height of parent materials BHT and BT-BMZ.

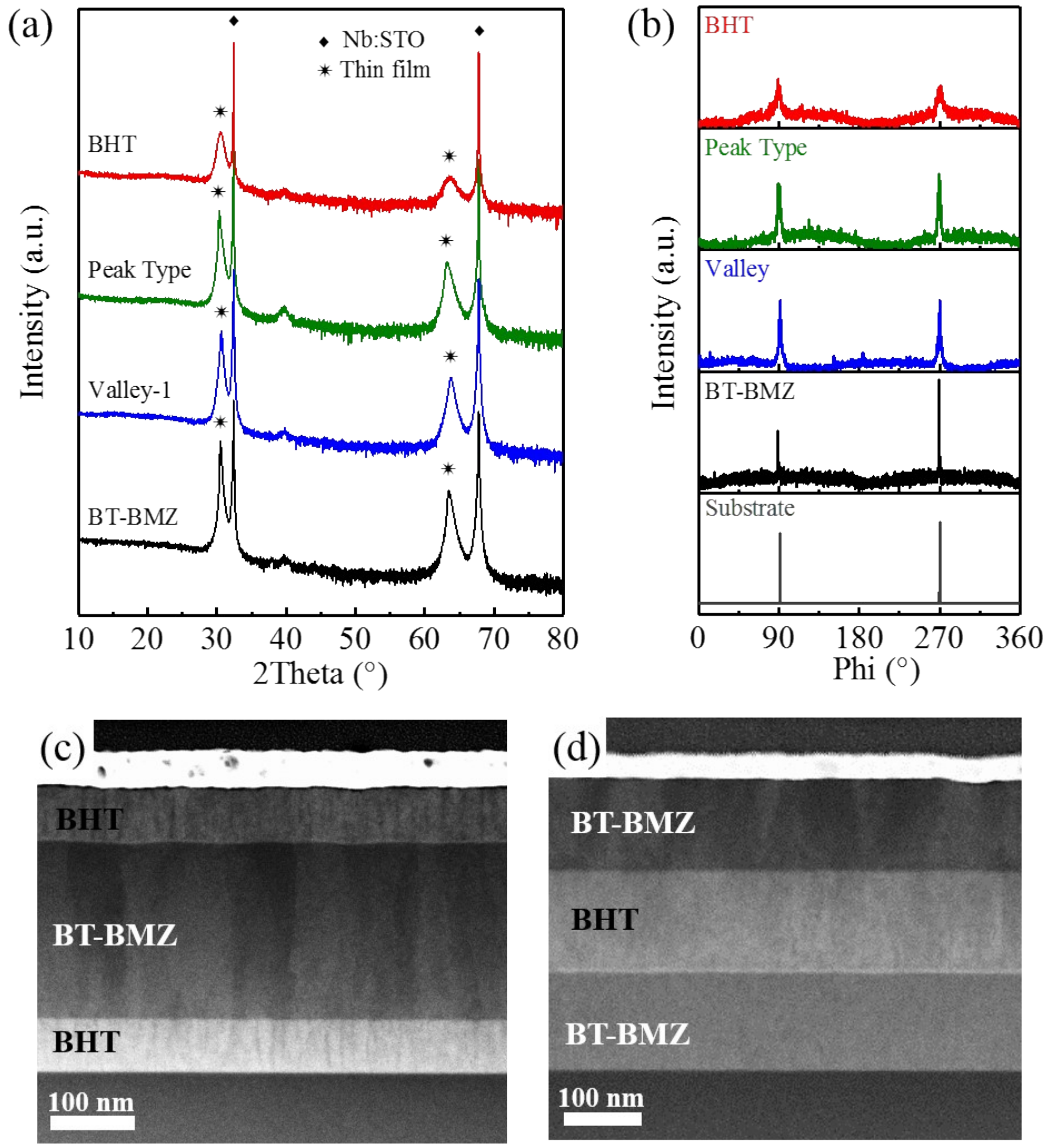

Fig S4 (a) XRD *theta-2theta* result of the BHT, Peak Type, Valley-1 and BT-BMZ films. **(b)** *Phi*-scan result of the BHT, BT-BMZ, Valley-1, Peak type thin films and corresponding substrate around. Cross-sectional STEM images of **(c)** the Peak Type and **(d)** the Valley-1 multilayer thin films.

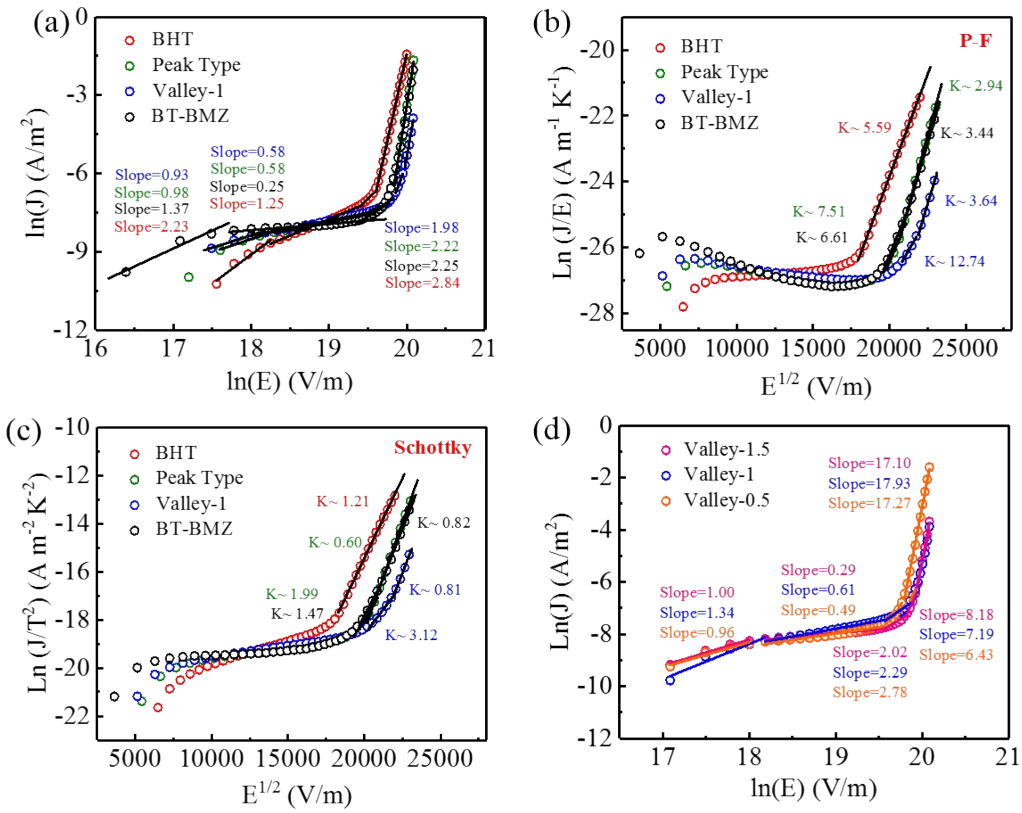

Fig S5 Fittings of leakage current density of the BHT, Peak Type, Valley-1 and BT-BMZ thin films based on conduction mechanism of **(a)** ohmic conduction and space charge limited conduction (SCLC), **(b)** P-F emission, and **(c)** schottky emission. **(d)** Fittings of leakage current density of the Valley-1.5, Valley-1, Valley-0.5 thin films based on conduction mechanism of Ohmic conduction and SCLC.

The first stage (0~0.84 MV/cm) of BHT thin films fitted slope closer to 2 like SCLC conduction mechanism. Considering the carrier of SCLC mechanism normally exceeds that of Ohmic mechanism, we supposed the defects in the films induce the “SCLC-like” behavior in the first stage.

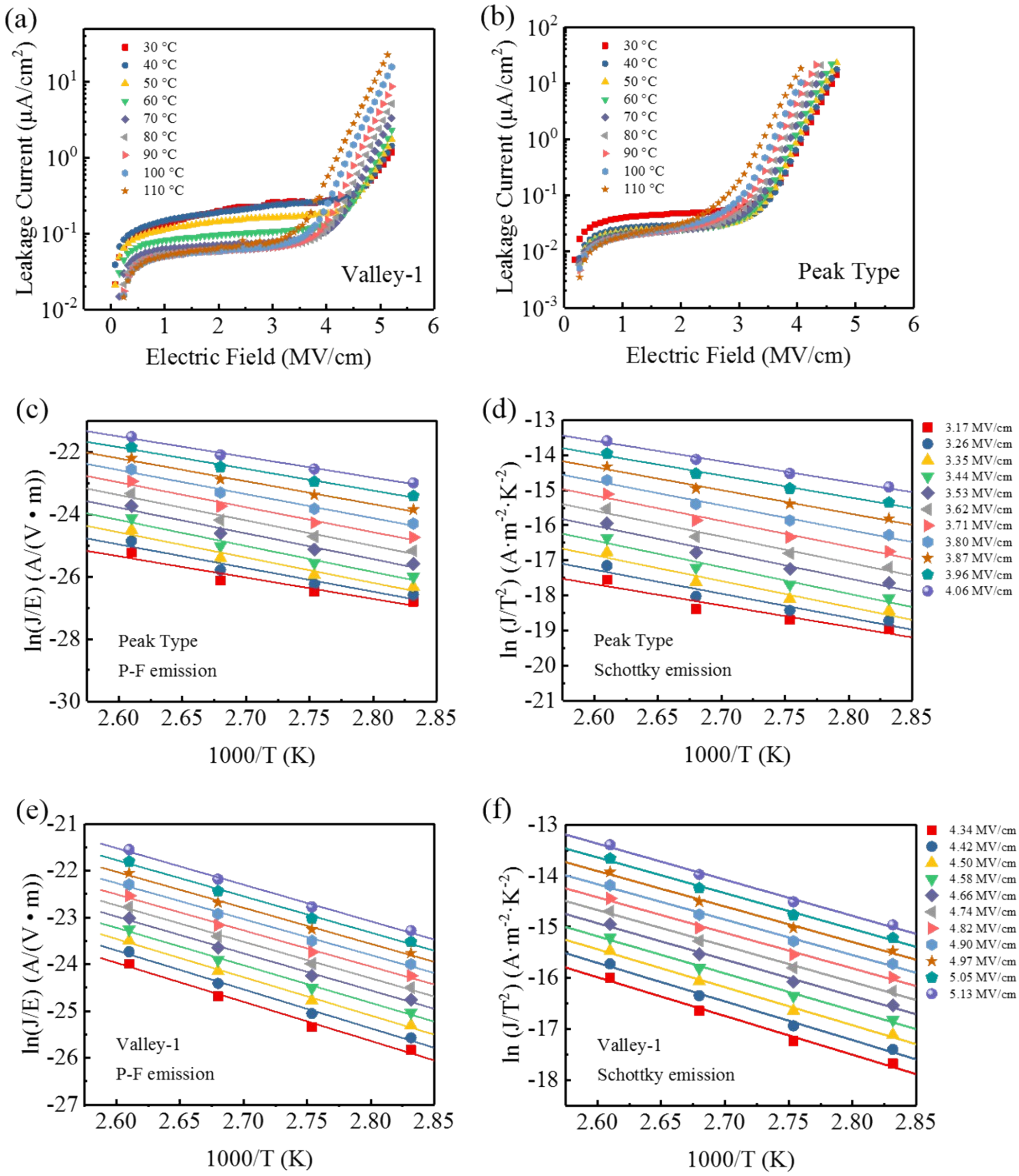

Fig S6 Leakage current density of **(a)** the Valley-1 and **(b)** Peak Type films as a function of electric field under different temperature. Linear fittings of the temperature-dependent leakage currents to extract thermal activation energies (E_a) based on **(c)(e)** P-F emission and **(d)(f)** schottky emission mechanisms.

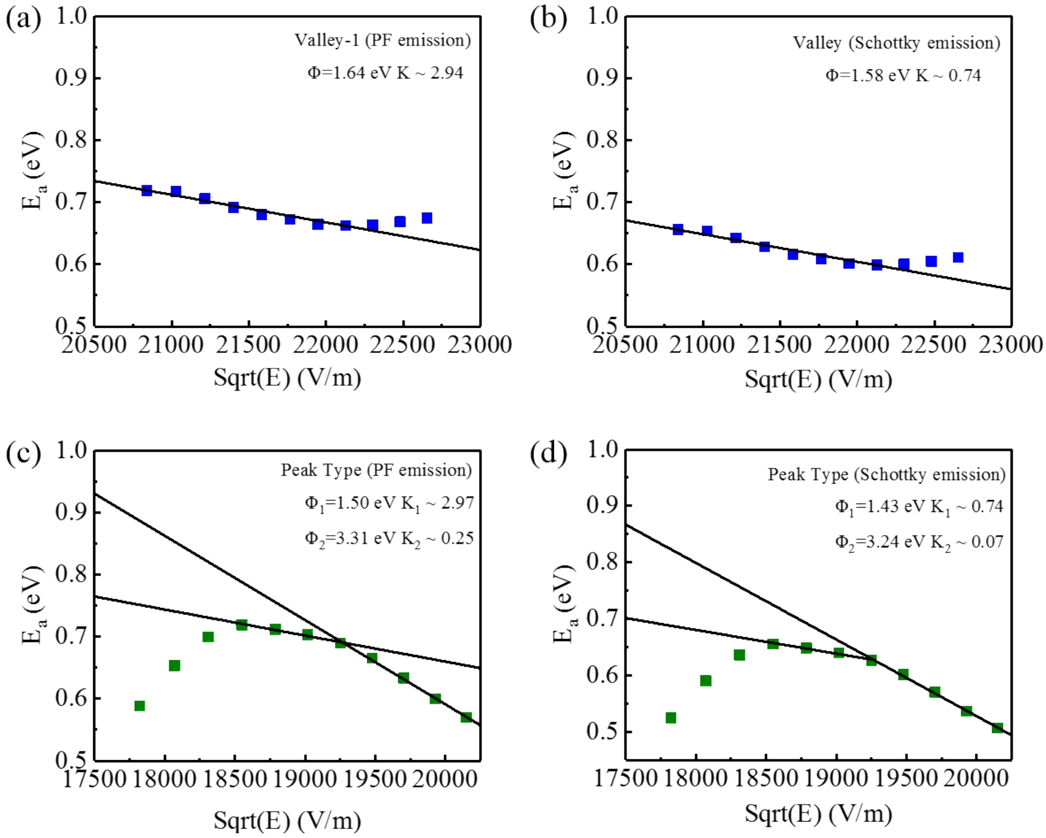

Fig S7 Plots of E_a values to extrapolate the barriers height $\Phi_{P\text{-}F}$ for **(a)** the valley-1 film, **(c)** the Peak Type film, and $\Phi_{Schottky}$ for **(b)** the valley-1 film, **(d)** the peak Type film.

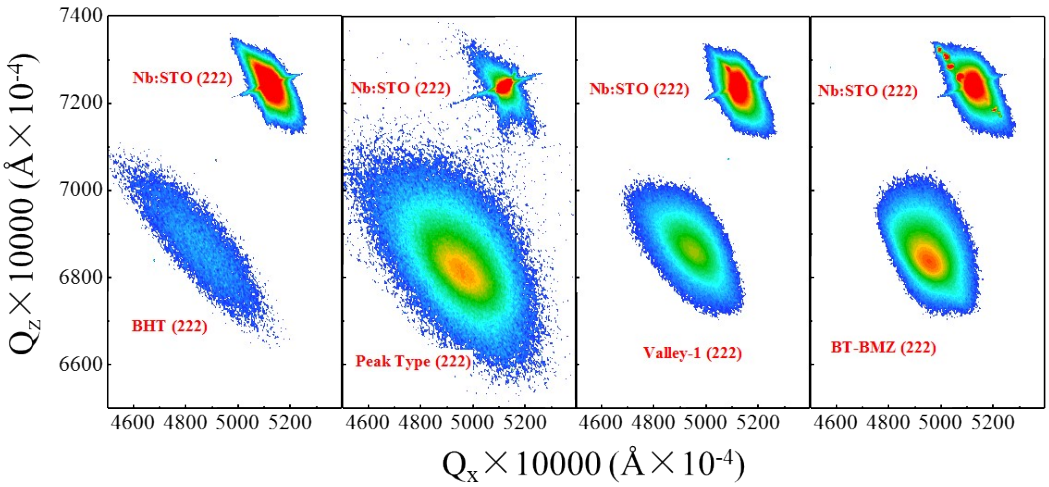

Fig S8 RSM results of (222) diffraction spots for the BHT, Peak Type, Valley-1 and BT-BMZ thin films.

We calculated the lattice constant in Table S1 according to their asymmetric RSM patterns in Fig S8. The out-of-plane lattice constant of Peak Type (2.94 Å) are larger than that of BHT (2.91 Å), BT-BMZ (2.92 Å) and Valley-1 (2.91 Å). The in-plane lattice constant are 3.905 Å for NSTO, 4.12 Å for BHT and 4.03 Å for BT-BMZ. The larger expansion out-of-plane lattice constant of Peak Type should be attributed to the larger in-plane lattice mismatch between BHT and NSTO. According their in-plane lattice constant BHT>BT-BMZ>NSTO, the valley-type multilayer thin film exhibit lower mismatch which could benefit to less defects in the Valley thin films than Peak Type. The less defects of Valley-1 can prevent the domain pinning of defect and benefits its maximum polarization.

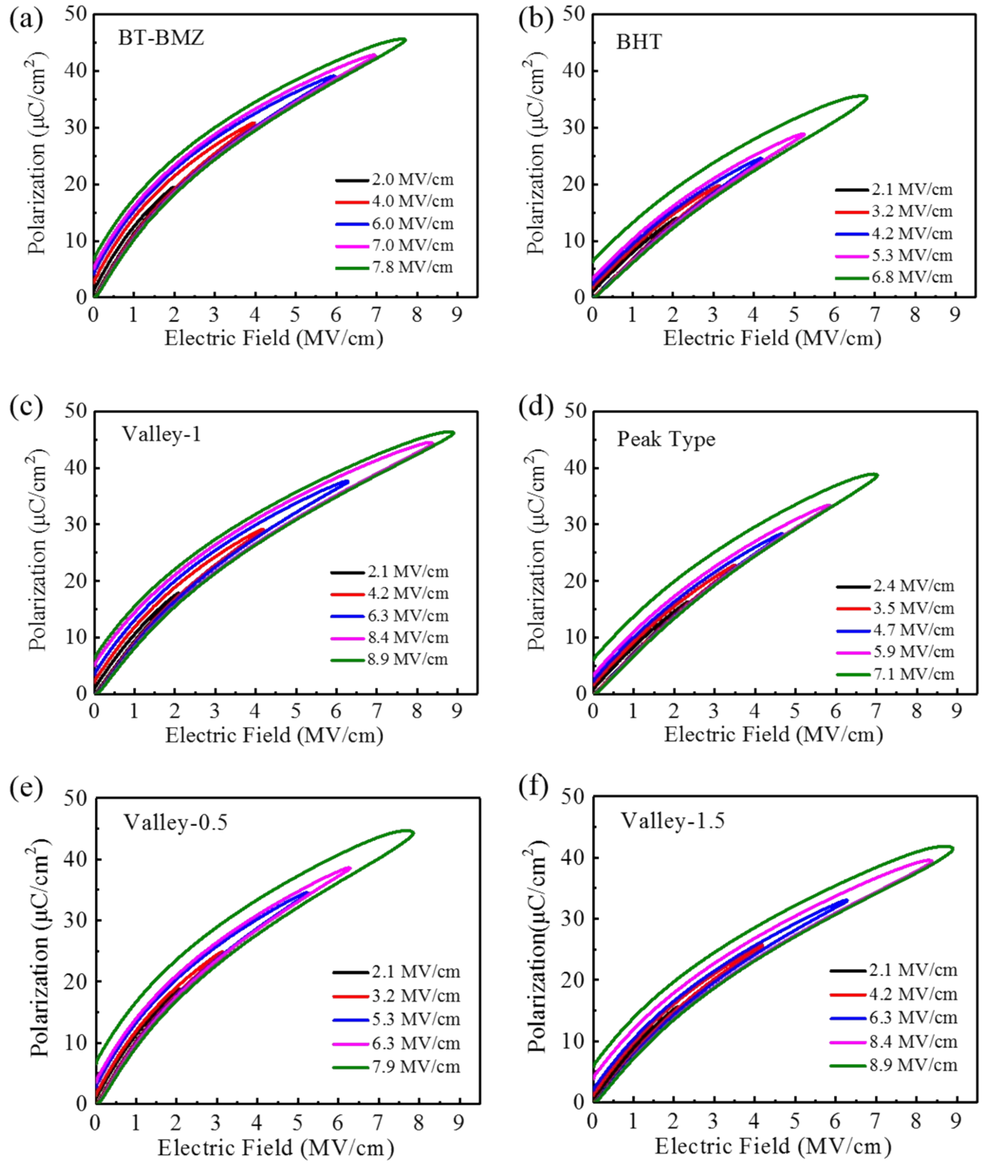

Fig S9 Unipolar *P-E* loops for the films of **(a)** BT-BMZ, **(b)** BHT, **(c)** Valley-1 **(d)** Peak Type **(e)** Valley-0.5 and **(f)** Valley-1.5 at 1 kHz under room temperature.

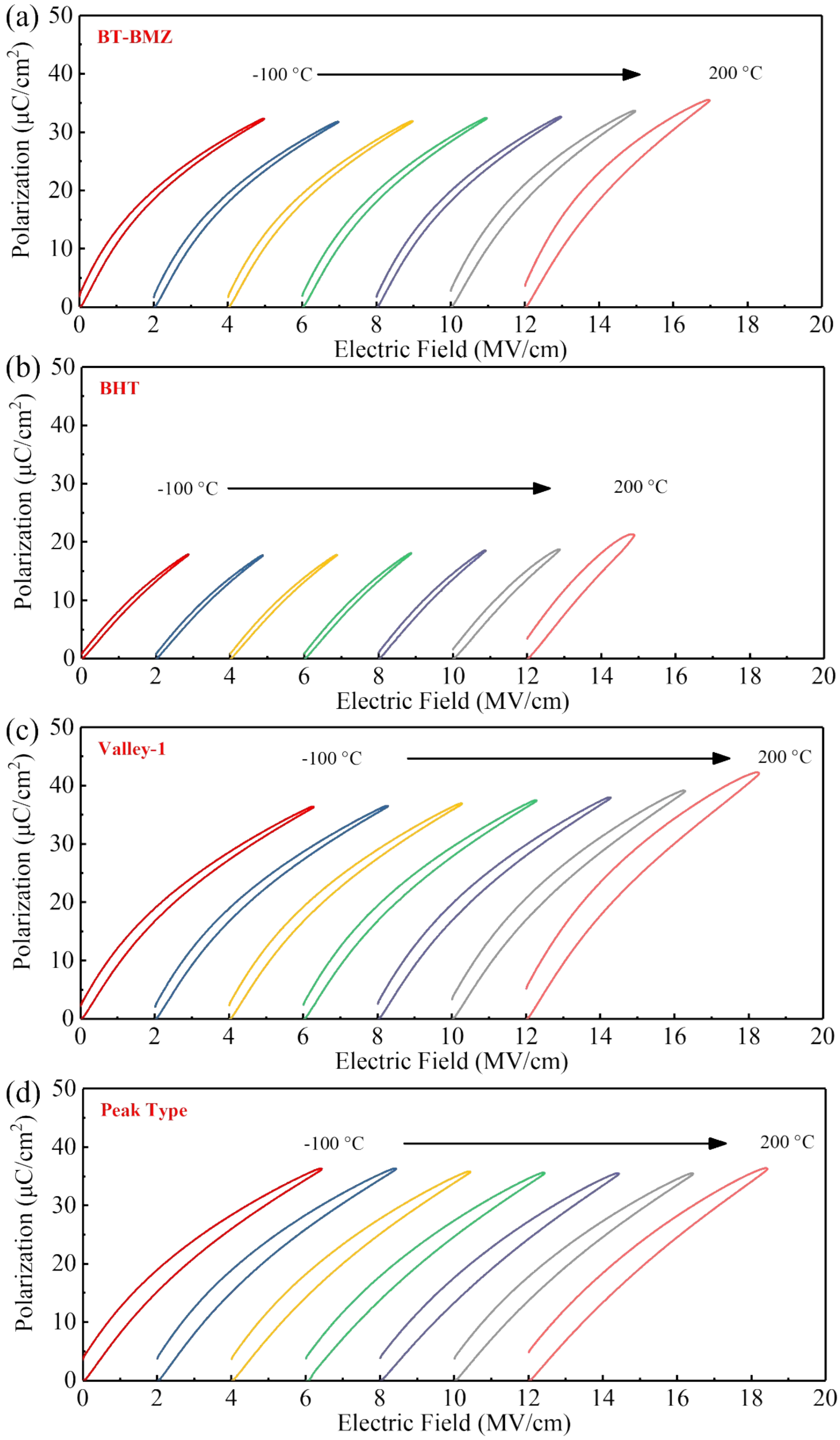

Fig S10 Unipolar *P*-*E* loops for the films of **(a)** BT-BMZ, **(b)** BHT, **(c)** Valley-1 and **(d)** Peak Type at 1 kHz at different temperature (-100 - 200°C).

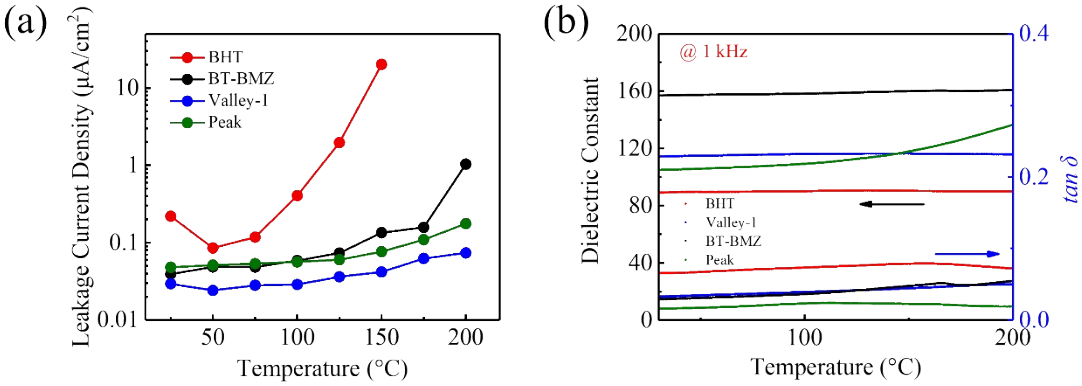

Fig S11 (a) Leakage current density as a function of temperature under 1.5 MV/cm for BHT, BT-BMZ, Valley-1 and Peak thin films. (b) Dielectric constant and dielectric loss of BHT, BT-BMZ, Valley-1 and Peak thin films as a function of temperature under 1 kHz frequency.

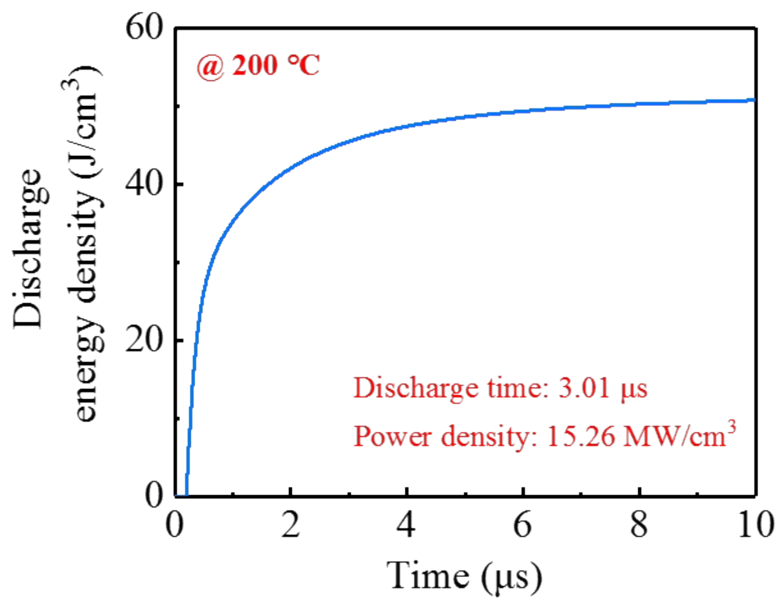

Fig S12 Discharge energy density as a function of time for the Valley-1 film (Charge electric field is 5.26 MV/cm, R_L=10 kΩ).

Table S1

	$d_{(001)}$ (Å)	$d_{(110)}$ (Å)
BHT	4.12	2.91
Peak Type	4.04	2.94
Valley-1	4.04	2.91
BT-BMZ	4.03	2.92

References:

[1] T.Y. Hu, C.S. Ma, J.Q. Fan, Y.L. Wu, M. Liu, G.L. Hu, C.R. Ma, C.L. Jia, Realizing high energy density and efficiency simultaneously via sub-grain modification in lead-free dielectric films, Nano Energy, 98 (2022) 9. https://doi.org/10.1016/j.nanoen.2022.107313.